



Investigating Temperature Variations of Solar Corona during Coronal Mass Ejections

Master's thesis submitted by

Dheeraj Vittal Shenoy

USN: 22MSRPH022

Under the guidance of

Mr. Sundar M. N.

and

Dr. Tanmoy Samanta

To

Department Of Physics and Electronics

School Of Sciences, JAIN (Deemed-to-be University)

Bengaluru

April 2024



Department Of Physics and Electronics
School Of Sciences, JAIN (Deemed-to-be University)
Bengaluru.

CERTIFICATE

This is to certify that the Masters thesis project titled "**Investigating Temperature Variations of Solar Corona during Coronal Mass Ejections**" has been the outcome of an original study carried out by **Dheeraj Vittal Shenoy** under the supervision of **Mr. Sundar M. N.** and **Dr. Tanmoy Samanta** towards the partial fulfilment of the requirements for the degree of M.Sc. Physics of JAIN (Deemed-to-be University).

This to further certify that the work reported herein does not form a part of any other thesis/dissertation, on the basis of which a degree, diploma or a certificate has been conferred upon this or any other student in the past.

Dr. Sudhakara Reddy

Head

Dept. of Physics and Electronics
JAIN (Deemed-to-be University)
Bengaluru

Mr. Sundar M. N.

Project Supervisor

Dept. of Physics and Electronics
JAIN (Deemed-to-be University)
Bengaluru

Tanmoy Samanta

Dr. Tanmoy Samanta

Project Co-supervisor

Assistant Professor
Indian Institute of Astrophysics
Bengaluru

Dr. Asha Rajiv
Director
School Of Sciences
JAIN (Deemed-to-be University)
Bengaluru

DECLARATION

I, **Dheeraj Vittal Shenoy**, hereby declare that this dissertation titled **Investigating Temperature Variations of Solar Corona during Coronal Mass Ejections** has been the outcome of an original study carried out under the guidance of **Mr. Sundar M. N.** and **Dr. Tanmoy Samanta** towards the partial fulfilment of the M.Sc. Physics degree of the JAIN (Deemed-to-be University) during the year 2023-2024. This study has not been submitted for any degree, diploma or certificate.

(Dheeraj Vittal Shenoy)

April, 2024

Bengaluru

ACKNOWLEDGEMENT

I would like to express my sincere gratitude to **Mr. Sundar M. N.** and **Dr. Tanmoy Samanta** for their invaluable guidance and support throughout my project. Their expertise has been instrumental in my success. I am truly grateful for their contributions and the knowledge I have gained under their mentorship.

I am also grateful to **Dr. Asha Rajiv**, Director, School of Sciences, **Dr. K. N. Varalakshmi**, Director, Centre for Research in Pure & Applied Sciences and **Dr. S. A. Hariprasad**, Dean Academics, JAIN (Deemed-to-be University) for providing us with this opportunity. I am thankful to **Dr. Sudhakara Reddy**, Head of the Department of Physics and Electronics and **Dr. N. Shanthi**, Program-Head, M. Sc. Programme, for their constant support and encouragement.

I thank **Dr. Chenraj Roychand**, Chancellor, **Dr. N. Sundararajan**, Pro-Chancellor, **Dr. Jithendra Kumar Mishra**, Registrar and **Dr. Raj Singh**, Vice-Chancellor, JAIN (Deemed-to-be University), for providing the required infrastructure and support without which this project would not have been possible.

I am grateful to all the faculty members, Mr. Arvind Krishnapur, Physics lab technician and Mr. Rajesh, Physics lab assistant for their kind support towards us.

(Dheeraj Vittal Shenoy)

April, 2024

Bengaluru

UNDERTAKING

I, **Dheeraj Vittal Shenoy** hereby give an undertaking that the data reported in this dissertation will not be used for any publication, conference presentation or for any industrial interaction without a written approval from the Project Supervisor and the Director, School of Sciences, JAIN (Deemed-to-be University).

(Dheeraj Vittal Shenoy)

April, 2024

Bengaluru

Contents

Abbreviations	1
1 Abstract	2
2 Introduction	3
2.1 Structure of the Sun	3
2.2 Solar Corona	4
2.3 Solar Flares	4
2.4 Coronal Mass Ejections (CMEs)	5
2.5 Stellar CMEs	6
2.6 Coronal Dimming	7
2.7 Instrument	7
3 Literature Review	11
4 Methodology	12
4.1 Data Analysis tools used	13
4.2 Event Selection	13
4.3 Data	15
4.4 Image Pre-Processing	15
4.5 DEM Analysis	16
4.5.1 Emission Measure	16
4.5.2 Differential Emission Measure	17
4.5.3 Differential Emission Measure Inversion	18
4.6 Data Analysis Procedure	19
5 Results	21

List of Figures

1	Structure of the Sun	3
2	Image of Solar corona during a total solar eclipse	4
3	Solar flare (4 th August 2011)	5
4	Filament and Prominence	6
5	AIA images of Coronal Dimming regions on the Sun	8
6	SDO Spacecraft	9
7	AIA Telescopes	10
8	AIA Telescope Layout	10
9	AIA Temperature Response Curves	11
10	Image of the Earth to scale of the 2012 August	14
11	SOHO/LASCO C2 images of the selected events	14
12	SOHO/LASCO C2 images with AIA 193 Åfilter	15
13	DEM image of Sun	20
14	Full Disk and Pointified Image of Sun	20
15	DEM Timeseries for August 2011 Event	21
16	DEM Timeseries for August 2012 Event	21
17	DEM Timeseries for October 2021 Event	22
18	DEM profile for 4 th August 2011 event	23
19	DEM profile for 31 st August 2012 Event	23
20	DEM profile for 28 th October 2021 event	24

Abbreviation	Full Form
SDO	Solar Dynamics Observatory
AIA	Atmospheric Imaging Assembly
HMI	Helioseismic Magnetic Imaging
EVE	Extreme ultraviolet Variability Experiment
SOHO	Solar and Heliospheric Observatory
LASCO	Large Angle and Spectrometric Coronagraph Experiment
EUV	Extreme Ultra Violet
DEM	Differential Emission Measure
JSOC	Joint Special Operations Command
FITS	Flexible Image Transport System
SSW	Solar SoftWare
IDL	Interactive Data Language
DN	Data Number

Table 1: List of abbreviations

1 Abstract

We investigate the temperature variations of solar corona during Coronal Mass Ejections through Differential Emission Measure (DEM) analysis of three CME events. We study the dimming of the corona due to the ejections of plasma, called as coronal dimming, and look into the temperature range of the coronal plasma that's most affected by this dimming. We study a filament eruption associated CME ejection and Groundlevel Enhancement CME event and study their affect on the coronal plasma temperature. Finally, we perform a Sun-as-a-star DEM analysis through pointification of full disk image of Sun to a point source and then look into the temperature variations of the point source.

2 Introduction

We briefly take a look at the structure of the Sun then proceed to eruptive events on the surface of the Sun like Solar flares, Coronal Mass Ejections, Stellar Coronal Mass Ejections, Coronal Dimming.

2.1 Structure of the Sun

Sun is divided into three regions, namely, interior region, visible surface and atmosphere. The interior region is further divided into core, radiative zone and convective zone. The **core** is the main fuel station for Sun, where nuclear fusion process is ongoing converting H to He. The radiations produced during the fusion process escapes through the surface as visible light. The **radiative zone** extends from the outer edge of the core to the base of the convective zone. Figure 1 shows the diagrammatic representation of the structure of Sun. The layer that separates the Sun's interior and it's atmosphere is called as **photosphere**. The outer atmosphere of the Sun is called the **corona**, which is a source of solar wind. The inner atmosphere of the Sun is known as the **chromosphere**. Because of the high hydrogen content, Sun appears red when viewed through a solar telescope, hence the name chromosphere.

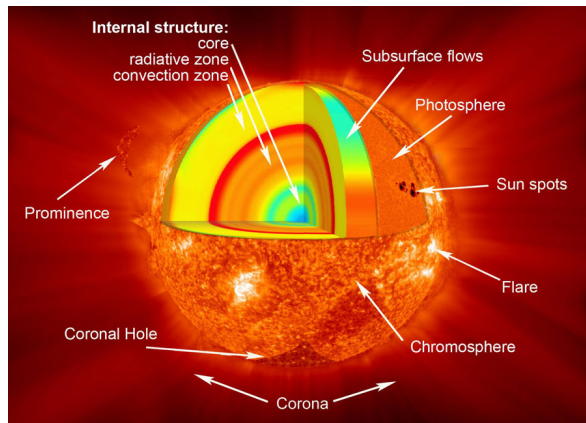


Figure 1: Structure of Sun. (Image credit: NASA)

The radiations produced in the core radiates slowly outwards through this region into the convective zone, taking more than about 170,000 years to radiate through this layer. The

convective zone is the region where the plasma, through the process of convection currents of heated and cooled gas, moves towards the surface.

2.2 Solar Corona

Outermost layer of the Sun's atmosphere is known as Solar Corona. It lies above the chromosphere and extends millions of kilometers into outer space. Corona can be easily viewed during solar eclipse (fig. 2), but can also be observed using a coronagraph. Coronagraph is a device that occults the disk of the Sun (similar to how moon occults the Sun during solar eclipse) thereby enabling easy coronal observations and analysis.

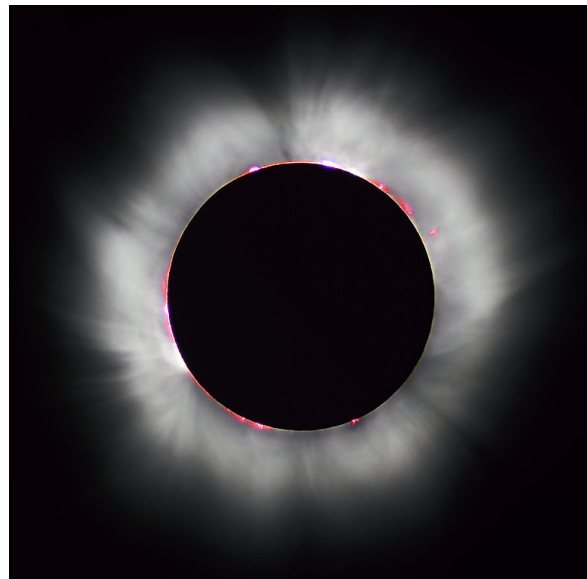


Figure 2: Image of Solar corona during a total solar eclipse. (Image credit: NASA)

The temperature of solar corona is of the order of million of degree kelvin. Because of this, it has unusual spectral features. The unusual spectral features have been explained by the existence of (Fe-XIV or Fe^{13+}). ([Aschwanden, 2006](#))

2.3 Solar Flares

Explosive phenomena that occur on the surface of sun are called as solar flares, caused by the reconnection of a sun's magnetic field lines. These flares are often accompanied by

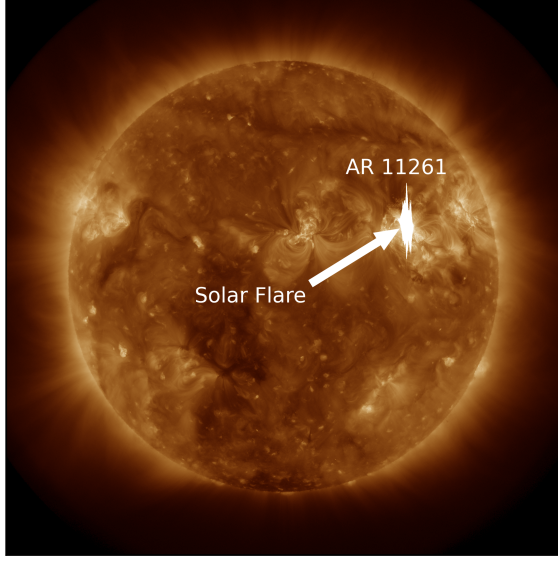
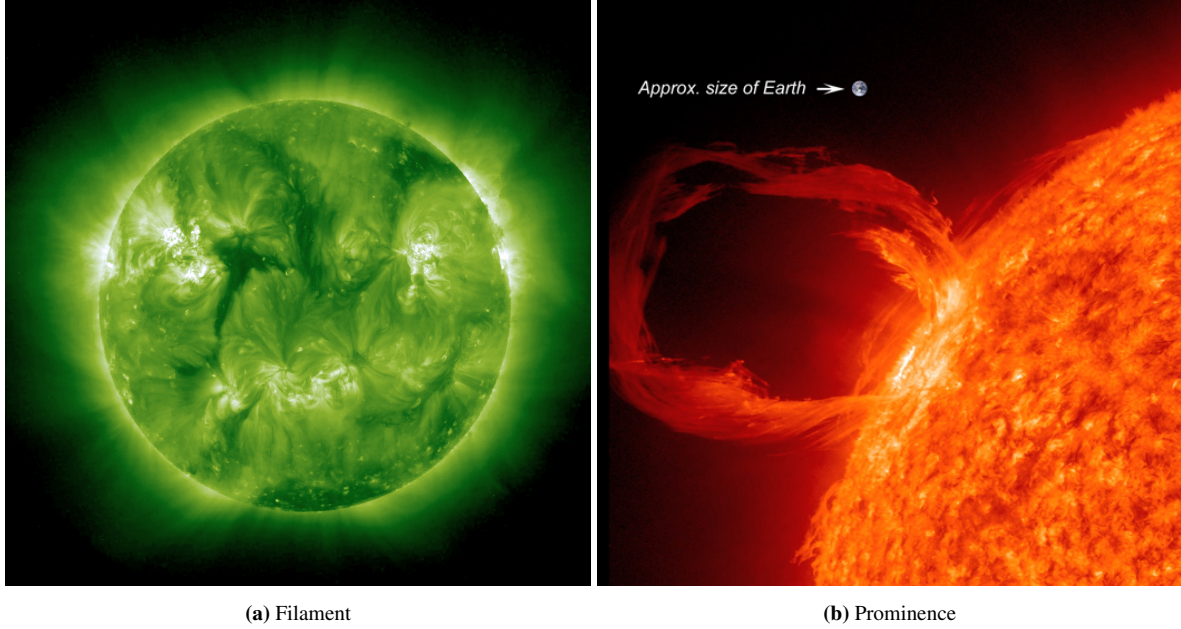


Figure 3: Solar flare event of 4th August 2011 originating from the Active Region AR 11261 observed through 193 Å AIA channel

filaments/prominent eruptions and Coronal Mass Ejections (CMEs). Flares are classified into two types: eruptive and confined. Eruptive events are the flares which are associated with CMEs and confined flares are those which are not associated with CMEs. Plasma and magnetic field structures sometimes extend outwards from the surface. These structures are called filaments/prominences. Filaments and prominences are fundamentally of the same physical properties, only difference is the angle at which it is observed. If plasma floats outside the solar limb, it is called prominence, it is called a filament if it is within the solar background otherwise section 2.3. Difference is in the type of spectrum obtained, which is Balmer lines in emission spectra in case of prominences and absorption lines in case of filaments. Loop-like structures of plasma stand out brightly against the dark background of space, these are prominences. An image of solar flare event of 4th August 2011 is shown in fig. 3.

2.4 Coronal Mass Ejections (CMEs)

CMEs are large plasma structures ejected from the solar surface to the heliosphere. They were first discovered in 1971 ([Gopalswamy, 2016](#)). They majorly affect the space weather,



(a) Filament

(b) Prominence

Figure 4: Figure 4a shows a U-shaped very long filament which was stable for a period of two days (6th - 7th February 2012) . Figure 4b is a prominence eruption seen in Extreme UV light on 30th March 2010 (credit: NASA).

causes interplanetary disturbances and shock waves. CMEs propagating towards the earth can disrupt the communication technologies like satellites. Filament eruptions and solar flares are often associated with CMEs. These energetic plasma have energy of the order of $10^{29} - 10^{32}$ erg and fast speeds even up to 3600 kms^{-1}

2.5 Stellar CMEs

Similar to solar flares, stellar flares maybe associated with CMEs, but it is not easy to detect or study them as there is no spatial resolution unlike Sun. CMEs accompanied by stellar flares are substantially larger in comparison to the ones observed on the Sun, and have been known to affect the exoplanets around the host stars (**Veronig et al., 2021**). Hence studying the CMEs is very crucial for future exoplanetary expeditions also. Indirect stellar CME detections have been explored with methods such as coronal dimming, blueshifted emission of chromospheric lines, X-ray, EUV and FUV dimming, Type-II and type-IV radio bursts etc (**Korhonen et al., 2016**).

2.6 Coronal Dimming

Coronal dimming is considered one of the promising signatures to detect the occurrence of stellar CMEs (**Namekata et al., 2022**). Regions with temporary dimming of plasma on the solar surface is seen after an eruptive event like CMEs in the EUV and soft X-ray wavelengths. This dimming observed is due to the mass loss in the corona after an eruptive event like CME (**Mason et al., 2014**). Dimming is most prominently observed in the 1-2 million K range of Sun's plasma of the quiet corona. Time series plot of irradiance value of Sun shows a prominent decrease after the event compared to the value before the event. This effect is known as Coronal Dimming. The probability of Coronal Dimming being associated with CMEs have been observed to be very high $P(Dim | CME) = 0.842$ in comparison to false alerts $P(Dim | !CME) = 0.167$. Probability of CMEs being associated with dimming ($P(CME | Dim) = 0.970$) is also very high(**Veronig et al., 2021**). Many studies have been done to get information about the underlying CME from the coronal dimming. The depth and slope of the dimming region in the light curve during CME events have been studied and empirical formulations have been done to get information about their mass and velocity (**Mason et al., 2016**).

2.7 Instrument

We are using Atmosphere Imaging Assembly (AIA) instrument of Solar Dynamics Observatory (SDO; (**Pesnell et al., 2011**)) for the Sun's spectral irradiance data. SDO is a space observatory launched by NASA on 2010 as a part of ‘Living With a Star’ (LWS) program. The spacecraft contains three instruments on board: Extreme Ultraviolet Variability Experiment (EVE), Helioseismic and Magnetic Imager (HMI), Atmospheric Imaging Assembly (AIA). We'll be focusing on the AIA instrument, since that is what we are using. AIA was built in partnership with Lockheed Martin Solar and Astrophysics Laboratory (LMSAL). AIA contains 4 cassegrain telescopes which are optimized to observe narrow bands in the EUV region. Each of the four f/20 telescope has a 20-cm primary mirror and an active

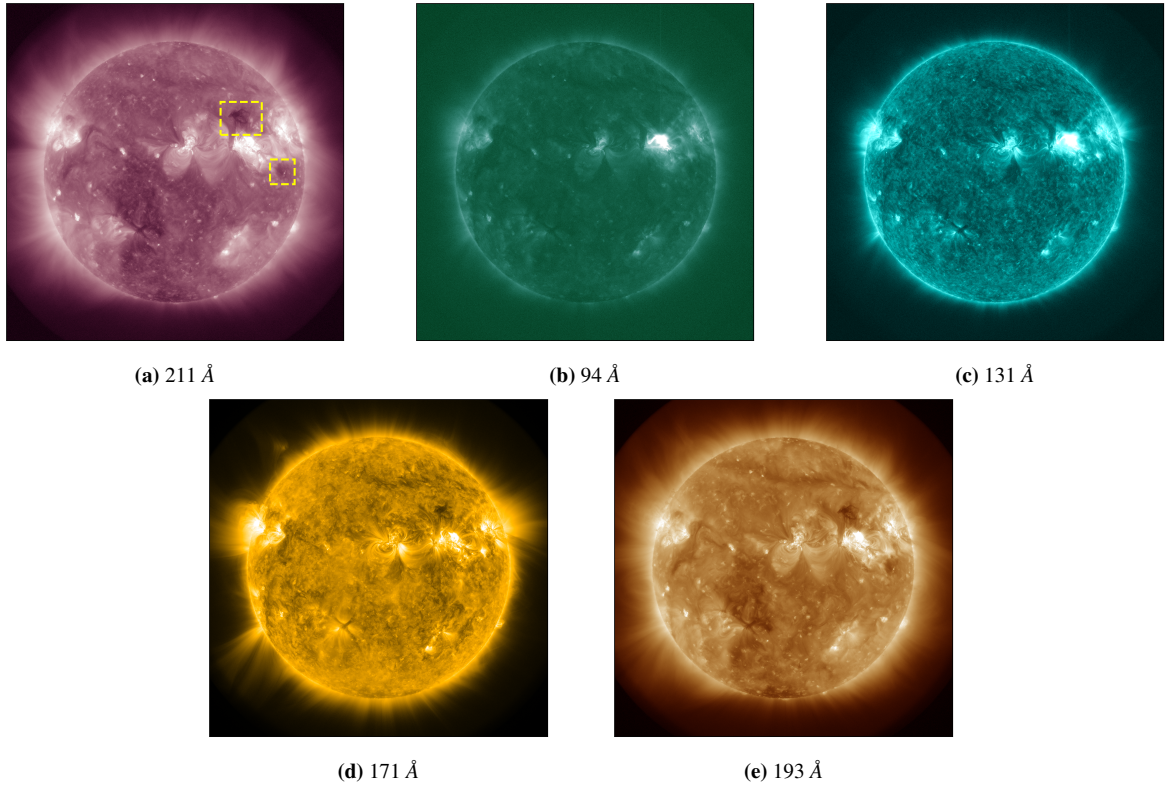


Figure 5: AIA images of the Sun depicting coronal dimming in five of the channels in the order: 211 Å, 94 Å, 131 Å, 171 Å, 193 Å. The two yellow dashed boxes depict the dimming region created because of the ejection of CME associated with the flare event of 4th August 2011 (dimming starts around 04:21 UT).

secondary mirror. The telescope is designed to prevent charged particles from reaching the Charge Coupled Device (CCD). Field of View (FOV) of each of the telescope is 41 arcmin in circular diameter. The mirrors have special multilayer coatings that are optimized to observe the selected EUV wavelengths of interest. Three of the telescopes have two different EUV bandpasses. The CCDs are back-thinned and back-illuminated with 4096×4096 pixels capturing capabilities. Each of the $12 \mu\text{m}$ pixel corresponds to 0.6 arcsec. The telescopes have a selector mechanism to choose the wavelength. AIA captures full-frame EUV image and one UV or visible-light image every 12 seconds. ([Lemen et al., 2011](#))

The different channels of AIA respond differently to the radiation of different temperature. The different channels of AIA along with its primary role, region of Sun's atmosphere it probes and temperature has been given in table 2. The response of the instrument to

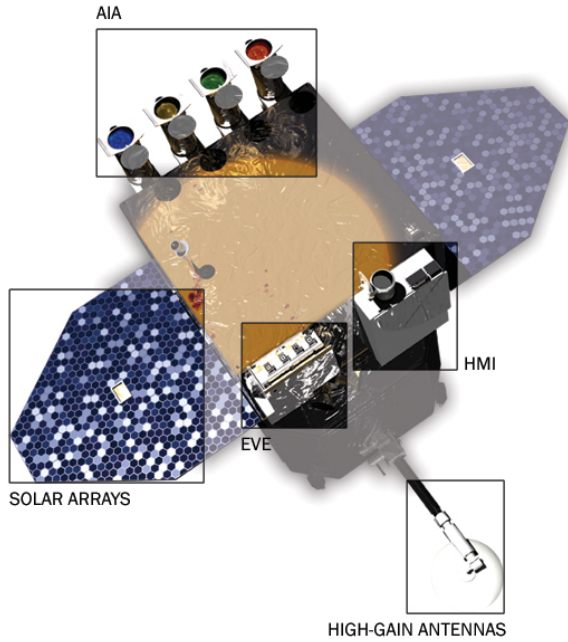


Figure 6: Solar Dynamics Observatory Spacecraft. Image obtained from <https://sdo.gsfc.nasa.gov/mission/spacecraft.php>

Band	Primary role, ion(s)	Region of Sun's atmosphere	logT[K]
4500 Å	Continuum	Photosphere	3.7
1700 Å	Continuum	Temperature minimum, photosphere	3.7
304 Å	He II	Chromosphere, transition region	4.7
1600 Å	C IV, continuum	Transition region, upper photosphere	5.0
171 Å	Fe IX	Quiet corona, upper transition region	5.8
193 Å	Fe XII, XXIV	Corona and hot flare plasma	6.1, 7.3
211 Å	Fe XIV	Active region corona	6.3
335 Å	Fe XVI	Active region corona	6.4
94 Å	Fe XVIII	Flaring regions	6.8
131 Å	Fe XX, XXIII	Flaring regions	7.0, 7.2

Table 2: AIA wavelength channels. Table obtained from <https://aia.lmsal.com/public/instrument.htm>



Figure 7: SDO AIA Telescope (Lemen et al., 2011)

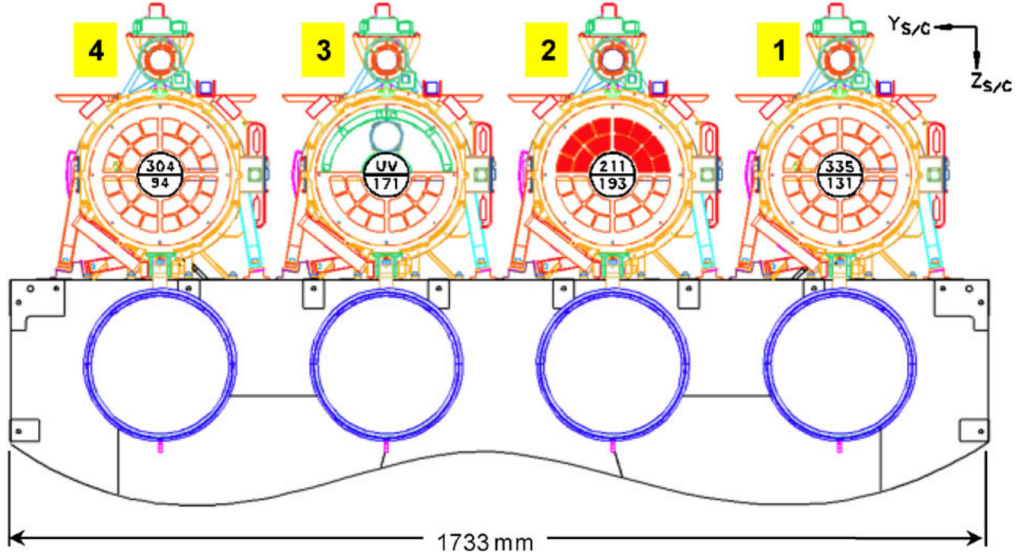


Figure 8: AIA Telescope Layout. Telescope 2 has an aperture blade to select between it's two wavelength channels. Rest of the telescopes rely on the filters in filter wheels to select the channel (Lemen et al., 2011)

different wavelengths and temperature is given by it's response curves, which are of two types, wavelength response curve and temperature response curves. Temperature response curves gives the information about the response of each of the channels with respect to the temperature of the radiation being received. Temperature response curves play a crucial role in DEM analysis. Figure 9 shows the response curves, which has been obtained using `aia_get_response.pro` procedure of SSW IDL.

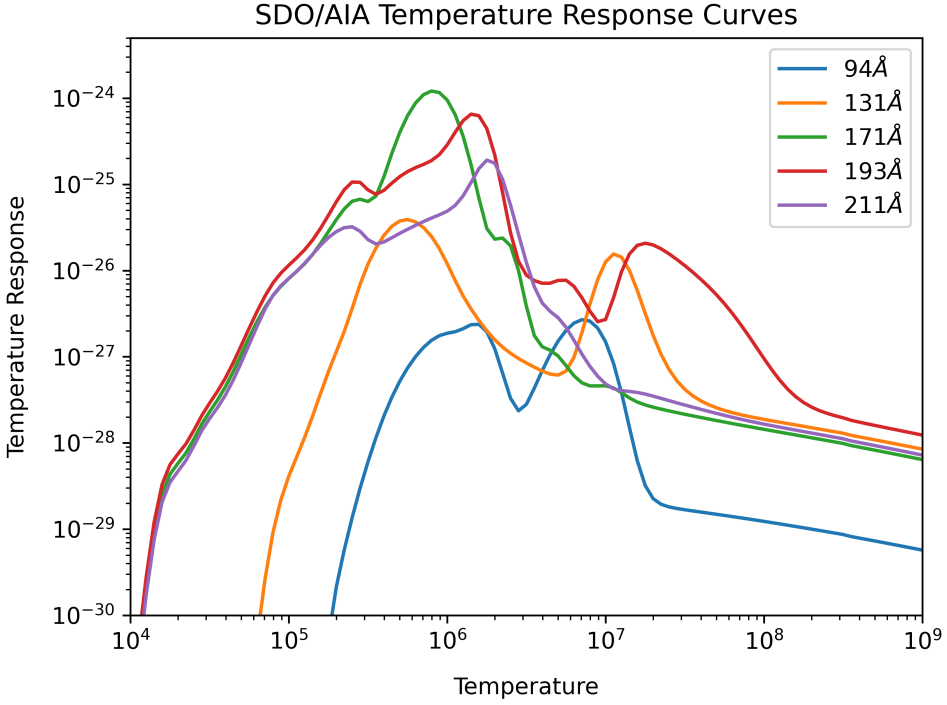


Figure 9: SDO/AIA Temperature Response Curves obtained using `aia_get_response.pro`. Curves corresponding to the five wavelength channels required for the DEM analysis has been plotted. Temperature has usual unit of [K] and temperature response function has the unit of [$\text{DN cm}^5 \text{s}^{-1} \text{pixel}^{-1}$]

3 Literature Review

The motivation for indirect detection of CMEs from Sun has led researchers to find out association of CMEs with eruptive events on the Sun like Solar flare, filament and prominence eruptions, coronal dimming associations with CME and vice-versa etc. About 73 % association of CME events with eruptive filaments has been observed ([Sinha et al., 2019](#)). It has been demonstrated that EM distributions from SDO/AIA data alone can overestimate the amount of high temperature ($\log T > 6.4$) plasma in the solar corona by a factor of 3-15 ([Athiray and Winebarger, 2024](#)). Coronal dimming phenomena have been extensively studied and many empirical formulations have also been derived to get information about the underlying CMEs like mass and velocity of the CMEs ejected by knowing the depth and slope of the dimming curve ([Mason et al., 2016](#)). The association of dimming

with a CMEs and association of CME with dimming has been observed to be very high ($P(Dim | CME) = 0.842$, $P(Dim | !CME) = 0.167$, $P(CME | Dim) = 0.970$) (Veronig et al., 2021). Sun-as-a-star analysis methods have been used widely for comparing and studying stellar and solar CMEs. Multi-temperature structure analysis of stellar active phenomena in spatially integrated spectra is allowed by the combination of H α and EUV lines, instead of single spectra analysis (Otsu and Asai, 2024). Redshifted components of stellar filament eruptions in Sun-as-a-star analysis in H α spectra may develop into CMEs (Otsu et al., 2022). Further studies into stellar CMEs connecting the CME mass and velocity to the stellar flare energy, leading to the conclusion that stellar CMEs are restricted in terms of their velocity due to the strong stellar magnetic fields and stellar wind drag (Moschou et al., 2019). One expects that the case of stellar CME in terms of its energetics and association to stellar flares will be a scaled version of the solar CMEs, but discrepancy has been found in terms of the ratio between the Kinetic energy of stellar CME to the stellar flaring energy not being anywhere close to being a scaled version of the solar case (Namekata et al., 2022).

4 Methodology

In this study, we wish to find a method of detecting signatures of CMEs on the Sun by converting it to a point source (hereafter referred to as **Pointifying**) and then inspecting if the signatures of the CMEs exist after the conversion and is similar to what was before the conversion. Pointifying the Sun roughly translates to converting Sun to a star, or placing Sun to a place that's distant from Earth/observer in comparison to the distance between us and the Sun (defined as astronomical unit ($1 \text{ AU} \approx 1.496 \times 10^8 \text{ km}$)) such that it appears as a point source. We then analyse and compare the irradiance from the point source Sun and the full disk Sun using DEM to see if they show similar signatures of CMEs. Typically, Sun-as-a-star analysis involves selecting a region of interest on the surface of the Sun, making the assumption that this is the only region that affects the event under study, and that there is no activity anywhere on the rest of the Sun's surface, and then integrating the parameter of interest over the entire Solar disk. This is again a rough approximation to an actual star.

In the following section, we discuss about the analysis tools used (section 4.1), selection of events (section 4.2), data used for the study (section 4.3), data pre-preprocessing (section 4.4), data analysis procedure (section 4.6).

4.1 Data Analysis tools used

We have made use of Python programming language for our analysis. We have made extensive use of the following libraries: Numpy, Scipy, Aiapy, Sunpy, Pandas, Matplotlib, Astropy, Natsort, Multiprocessing, Datetime, Moviepy. In addition, we have used the RML method code for DEM analysis, as mentioned in (Massa et al., 2023). We have made use of SSW IDL for obtaining the temperature response curves for AIA. For visual inspection of the CME events, we have used JHelioViewer software. For quick inspection of the data, we have used FITSExplorer¹, a software created as a side project by D. V. Shenoy.

4.2 Event Selection

We have chosen three CME events that have erupted on 2011 August 04, 2012 August 31 and 2021 October 28. The Solar and Heliospheric Observatory's (SOHO) Large Angle and Spectrometric Coronagraph Experiment (LASCO) C2 (SOHO/LASCO) images of the CMEs obtained from the SOHO/LASCO CME catalog (https://cdaw.gsfc.nasa.gov/CME_list/) are given in fig. 11 and fig. 12. Brief description of the events is given below:

1. **2011 August 04:** This event has been referred from (Mason et al., 2016) in which it is the 20th Event. The event started at around 04:12 UT. This event occurred from the source location N19W36 associated with the active region AR 11261.
2. **2012 August 31:** This CME event was associated with a long filament eruption and it erupted around 19:49 UT. The CME associated with the filament travelled at over 900 miles per second.

¹link to the github repo: <https://github.com/dheerajshenoy/FITSExplorer>

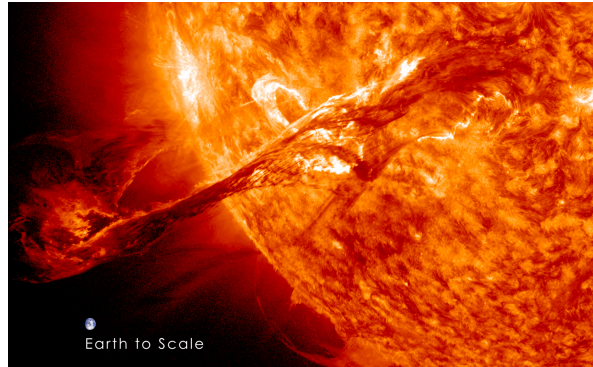


Figure 10: Image of the Earth to scale with the filament eruption of 31st August 2012. Image credit: <https://svs.gsfc.nasa.gov/11095>

3. **2021 October 28:** This is an example for rarely occurring ‘ground level enhancement’ event. During such an event, particles from the Sun are energetic enough to pass through the magnetic sheath that surrounds Earth and protects us from low energy solar outbursts. This was only the 73rd ground level enhancement since records began in the 1940s, and none have been recorded since ([Klein et al., 2022](#)). The event occurred around 15:17 UT. The flare associated with the CME was an X1.1 class flare originated from the active region AR 2887.

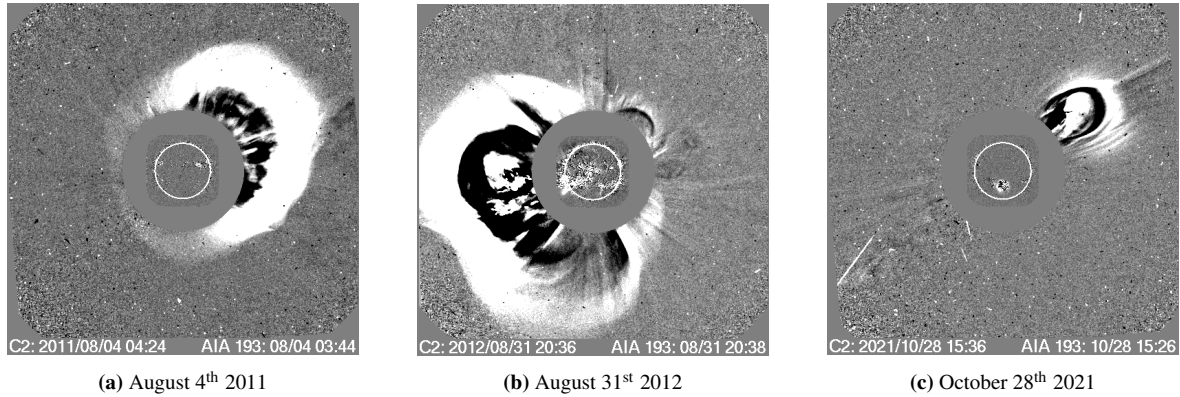


Figure 11: SOHO/LASCO C2 images of the three selected events

We have used 10 hours of data for the first two events, and about 7 hours of data for the third event. All three event data are at 2 minute cadence.

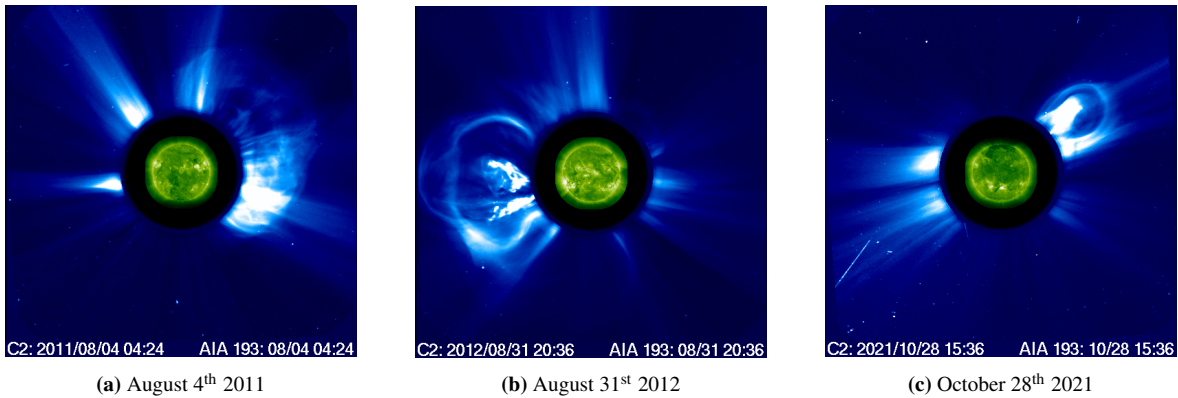


Figure 12: SOHO/LASCO C2 AIA 193 Åfilter images of the three selected events

4.3 Data

The SDO/AIA data is accessed through the JSOC portal (<http://jsoc.stanford.edu>) and required event data is obtained through the service. Event data consists of FITS files of Sun’s image for the selected wavelength bands. For our analysis, we have used 5 channels: 94 Å, 131 Å, 171 Å, 193 Å and 211 Å. The remaining channels probe the Sun’s surface temperature that is greater than what is required for our analysis. Also, the 335 Å channel has been excluded because of it’s relatively weak temperature response at any temperature which affects the RML method used for the DEM analysis ([Massa et al., 2023](#)).

4.4 Image Pre-Processing

The downloaded FITS data files are 4096×4096 pixels in dimension. Data downloaded from the portal is level 1, which has been flat-fielded and processed to remove bad pixels and spikes (only for EUV channels), but not registered to preserve precise pixel values. As different channels of AIA have different roll angles, multi-wavelength analysis of any kind with level 1.0 data is problematic. Also, the pointing information contained in the headers of these FITS images will not be accurate, as it would have undergone changes compared to the information stored when the image was created. As mentioned in the SDO Data Analysis Guide (REFERENCE REQUIRED), we have to use `aia_prep.pro` function in Solar Software (SSW) IDL to correct or prepare the data used. The images are downsampled from

their original 4096×4096 pixel dimension to 512×512 pixels using sunpy as obtaining DEM solutions for the 4k dimension would be really time consuming and unnecessary as we are comparing full disk and point source DEM solutions.

The **aiapy** library is used to carry out the necessary procedure like ‘**Pointing correction**’ and ‘**Registration**’ as mentioned in the documentation of aiapy, to convert level 1 data to level 1.5. Pointing correction updates the keywords in the header of the FITS file to the latest information and Registration rotates, scales and translates the image so that the Solar north is aligned with the solar north and each pixel is 0.6 arcsec cross, and the center of the Sun is at the center of the image. Now, after this calibration, the images are good for multi-wavelength analysis. Finally, the images are normalized with respect to their exposure time. This is done because the images are captured under different lighting conditions or exposure settings, which leads to incorrect analysis when performing a multi-wavelength comparison. Without this, differences in brightness due to varying exposure times could distort interpretations and analysis.

4.5 DEM Analysis

Direct analysis of light curve might seem like a good choice as the effects of CMEs are seen in light curves too. But, light curve doesn’t have any information about the temperature of the plasma that is being expelled. Information regarding the temperature can be derived using Differential Emission Measure (DEM) solutions obtained using the images of Sun.

4.5.1 Emission Measure

Emission measure (EM) is a quantity used in astrophysics to describe the amount of emitting material along the line of sight in a particular volume, usually in the context of a hot or ionized gas, such as a stellar atmosphere. It provides a measure of the emission intensity of a given region at various temperatures. Emission measure is expressed in units of cm^{-3} or cm^{-5} , representing the number of electrons emitting radiation per unit volume or per unit

area, respectively.

Emission measure is related to the number density of electrons n_e in a volume dV of plasma, in a particular temperature range T_1 and T_2 , along the line of sight, is given by,

$$EM = \int_{T_1}^{T_2} n_e^2 dV \quad (1)$$

Emission measure is a crucial parameter in understanding the energetics and physical conditions of a plasma, such as those found in stars, galaxies and other astrophysical environments. In the context of the Sun, the emission measure is often used to study the solar corona, helping us to understand the distribution of temperatures and the processes governing the heating of the outer solar atmosphere.

4.5.2 Differential Emission Measure

Differential Emission Measure (DEM) is used to describe the distribution of emitting material at different temperatures in a given volume. It is a measurement of the amount of plasma at various temperatures per unit volume along the sight. DEM helps us understand how much material is present at different temperature in stellar atmosphere. This is crucial for studying the physical conditions and processes occurring in stellar atmospheres. DEM is usually expressed in units of $cm^{-5}K^{-1}$, representing the number of particles emitting radiation at a particular temperature per unit volume.

$$DEM = f(T) = \frac{d}{dT} EM = n_e^2 \frac{dV}{dT} \quad (2)$$

The integral of $DEM(T)$ over a finite temperature range is called as the emission measure. This quantity helps to understand the thermal structure of a stellar atmosphere, providing insight into the distribution of temperatures and the heating mechanisms that operate in a particular region. DEM arises from certain aspects of coronal emission line. Optically thin property of corona, scaling of emission line intensity with density squared n^2 (for most lines)

and temperature response function, $R(T)$, that peaks at certain temperature for each of the lines.

If $R(x) \equiv R(T(x))$ is the temperature response function, then, line intensity along the line of sight can be written as,

$$I \propto \int_{LOS} n_e^2(x)R(T(x)) dx \quad (3)$$

From a *DEM*, parameters like plasma density, thermal X-ray flux, thermal energy and weighted temperature emission measure etc. can be estimated (**Su et al., 2018**). In solar research, DEM aids in understanding the Sun's atmosphere, while in stellar astrophysics, it contributes to characterizing other stars, enhancing our knowledge of stellar diversity and evolution (**Namekata et al., 2023**).

4.5.3 Differential Emission Measure Inversion

DEM inversion refers to the process of determining the physical conditions of the plasma from observed coronal emission line data. Radiation emitted by the plasma is observed at different wavelengths using spectroscopic techniques. The observed data is then used to construct the DEM, which represents the distribution of emitting material at different temperatures in the stellar atmosphere. Next, the inversion process is employed, which is basically reconstructing the DEM, thereby helping us to determine the underlying temperature distribution which gave rise to the observed emission line intensities. Then different computational techniques can be employed to fit theoretical models of the emission at different temperatures to the observed data. The best fit model then provides the information about the temperature distribution of the plasma.

Many DEM inversion techniques have been developed over the years: basis pursuit technique (**Cheung et al., 2015**), fast iterative regularized method (**Plowman et al., 2013**), iterative SITES method (**Morgan and Pickering, 2019**), regularized method (REG) (**Hannah and Kontar, 2012**), regularized maximum likelihood (RML) method (**Massa et al., 2023**)

etc. We will be making use of the RML method, as it has been found to be a good approximation to the actual DEM profiles and is performant in comparison to the other methods.

4.6 Data Analysis Procedure

After calibration (registering, pointing correction and exposure time normalization), the image data is fed to the RML code (2023) which returns the DEM solutions for the desired temperature range. We choose a temperature (logarithm) range of $\log T[K] = [5.85, 6.4]$ which translates to temperature of $10^{5.85} \approx 7 \times 10^5 K$ to $10^{6.75} \approx 5.6 \times 10^6 K$. The function `rml_dem` takes the following inputs: array containing the AIA data (DN/s), array of uncertainties of AIA data (DN/s), exposure time value for each AIA channel (s), array containing the temperature response function for each channel ($DN \text{ cm}^5 \text{ pixel}^{-1} \text{ s}^{-1}$), array containing the value of log base 10 of the center of each temperature bin, array containing the value of the width of base 10 logarithm of the temperature bins. The function returns an array containing the values of the reconstructed DEM profiles. The returned solutions will be spaced according the temperature spacing of the response function array fed to the solver. The solutions obtained can be plotted to look at the emission measure distribution as shown in fig. 13.

Next step is to generate the point source from the full disk, which we refer to as “Pointification”. This involves the conversion of the full disk image of Sun to a point source, which mimics a distant star. The original image of 4096×4096 pixels dimension is averaged and new image having 512×512 pixels dimension is created with the pixel value at (256, 256) of the image (midpoint of the image) equal to the calculated average image pixel value. The average values of 4096×4096 pixel image dimension has been considered and not the 512 one so as to not allow the errors due to the resampling of the image affect the average pixel intensity value significantly. Figure 14 shows the result of pointification procedure. After pointification, DEM profile is reconstructed from these images. These act like DEM profiles of a point source/star.

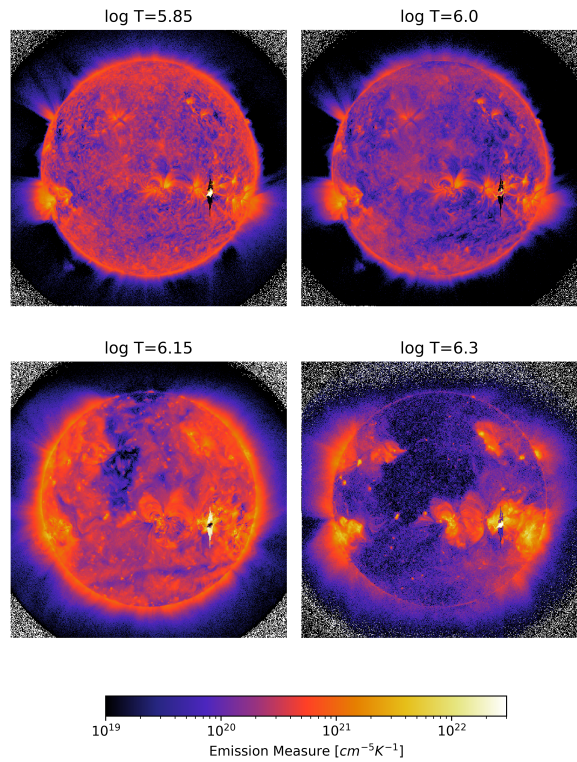


Figure 13: DEM of Sun during the flaring event on 4th August 2011. The artifacts at the corners of the image is due to the diffraction of light in the telescope of AIA

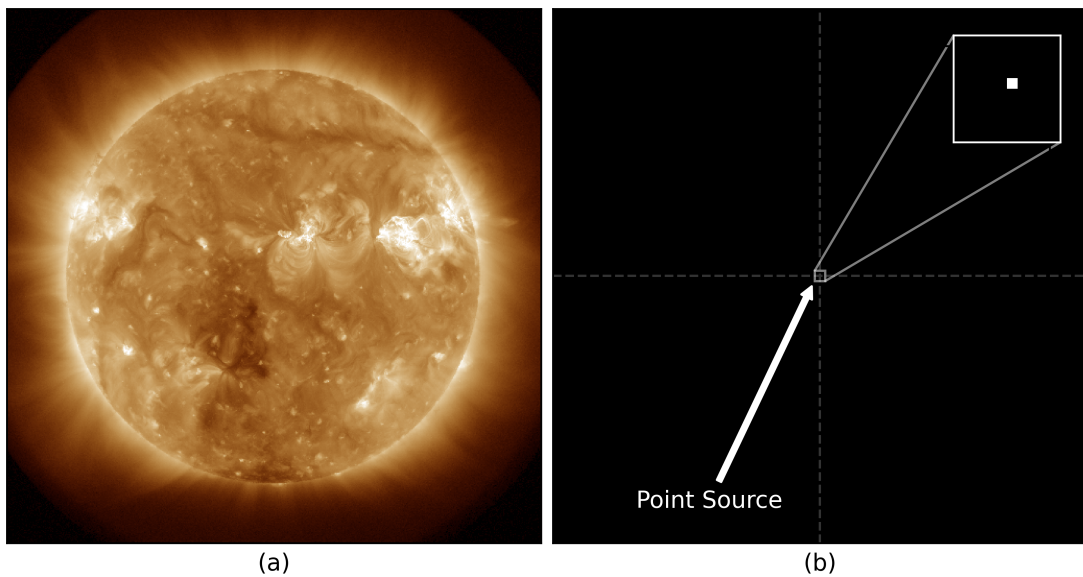


Figure 14: (a) shows the full disk image of Sun in the 193 Å channel, (b) shows the image after pointification.

5 Results

Figure 15, fig. 16 and fig. 17 shows the timeseries plot of DEM for the three events. The time series plot is calculated by averaging the acceptable DEM solutions obtained for each image over three consecutive temperature range (i.e averaging the solutions for 5.85, 5.9 and 5.95 etc.). Blue curve corresponds to the full disk DEM and red curve corresponds to the point source DEM. The temperature range above $\log T = 6.75$ has been omitted as no correlation was found between point source and full disk.

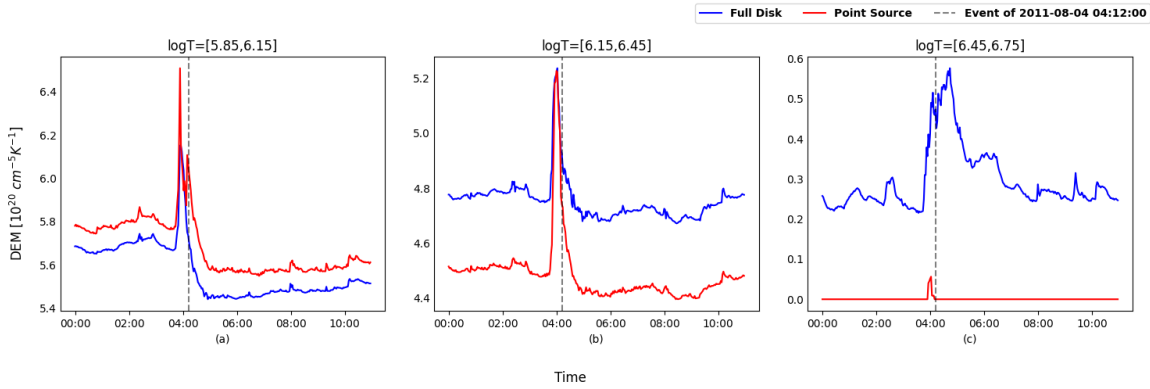


Figure 15: Timeseries of DEM for 4th August 2011 Event.

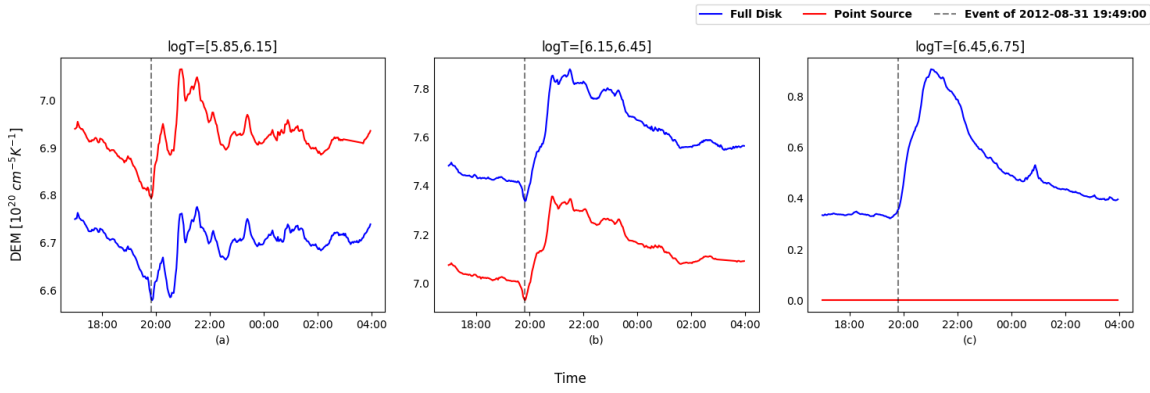


Figure 16: Timeseries of DEM for 31st August 2012 Event

In fig. 15(a) and fig. 15(b), we can observe the coronal dimming or decrease in the DEM value after the event spike. But, in fig. 15(c) no dimming is observed. Dimming is the most prominent in $\log T = [5.85, 6.15]$. The sudden increase in the DEM curve is due to

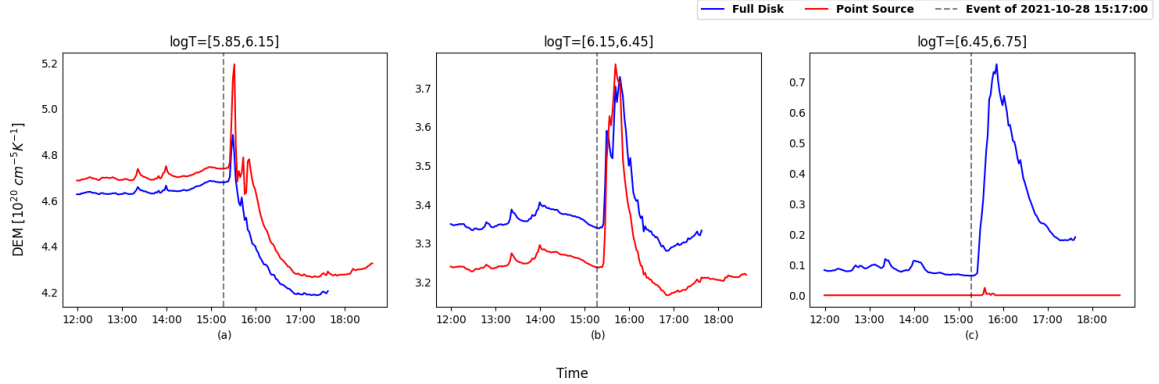


Figure 17: Timeseries of DEM for 28th October 2021 Event

the solar flare which is associated with the CME. There is very high correlation for the first two temperature ranges, but there is little to no correlation in the DEM profiles of the full disk and point source for the temperature range $\log T = [6.45, 6.75]$. For temperature ranges greater than $\log T = 6.45$, the correlation is almost 0. We make use of Pearson's Correlation coefficient (eq. (4)) to find out the amount of correlation between the point source and full disk DEM, for which we use `pearsonr` function from the `scipy` library in Python. The pearson correlation coefficient r between two datasets x and y is calculated using the formula,

$$r = \frac{\sum(x_i - \bar{x})(y_i - \bar{y})}{\sqrt{\sum(x_i - \bar{x})^2 \sum(y_i - \bar{y})^2}} \quad (4)$$

Event	Pearson Correlation Coefficient		
	$\log T = [5.85, 6.15]$	$\log T = [6.15, 6.45]$	$\log T = [6.45, 6.75]$
4 th August 2011	0.9449	0.9767	0.2190
31 st August 2012	0.7027	0.9885	0.2079
28 th October 2021	0.9555	0.9577	0.2578

Table 3: Correlation between Point source and Full Disk DEM

We see a discrepancy in the value of DEM between the point source and full disk average values. This could be due to the error induced during the DEM profile reconstruction,

instrumental errors, error incurred during the resampling or reduction of image dimension from 4096×4096 pixels to 512×512 and it could also be due to averaging error. The dataset length is not equal in some of the case as invalid or small DEM solution values have been removed.

The temperature distribution of the plasma at different sections of an event can be studied through its DEM profile (DEM profile is a plot of $\log T$ vs DEM). The DEM profiles before, during and after the event has been shown in fig. 18, fig. 19 and fig. 20 for the events of 4th August 2011, 31st August 2012 and 28th October 2021 respectively.

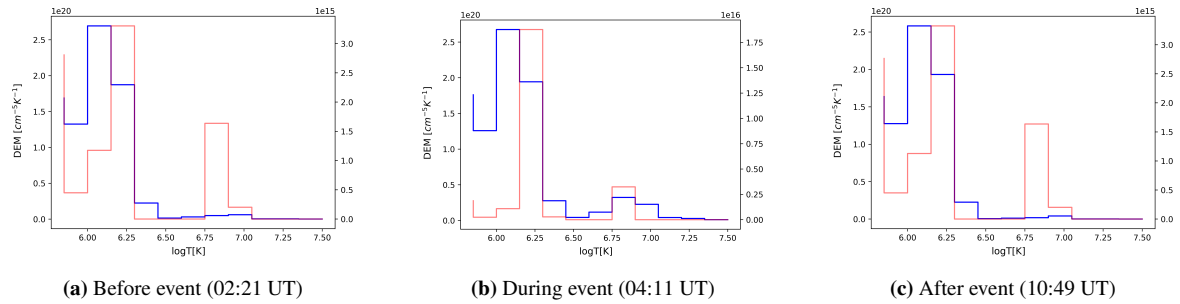


Figure 18: DEM profile before, during and after the flaring event of 4th August 2011. The red and blue curves correspond to point source and full disk source respectively.

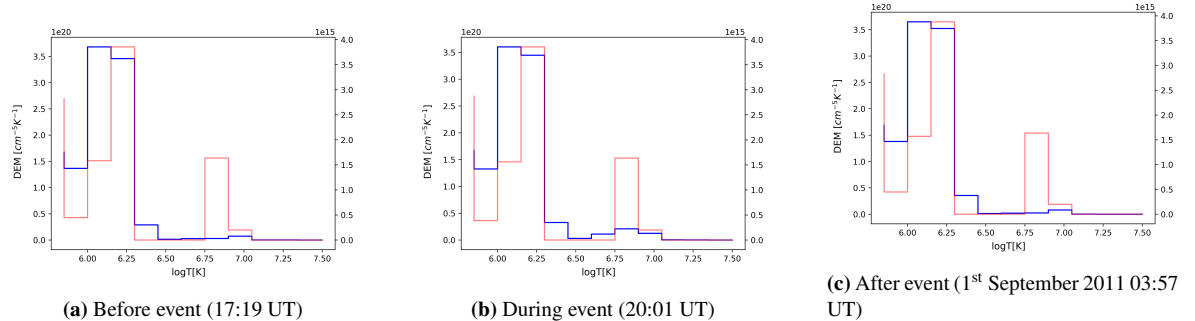


Figure 19: DEM profile before, during and after the flaring event of 31st August 2012. The red and blue curves correspond to point source and full disk source respectively

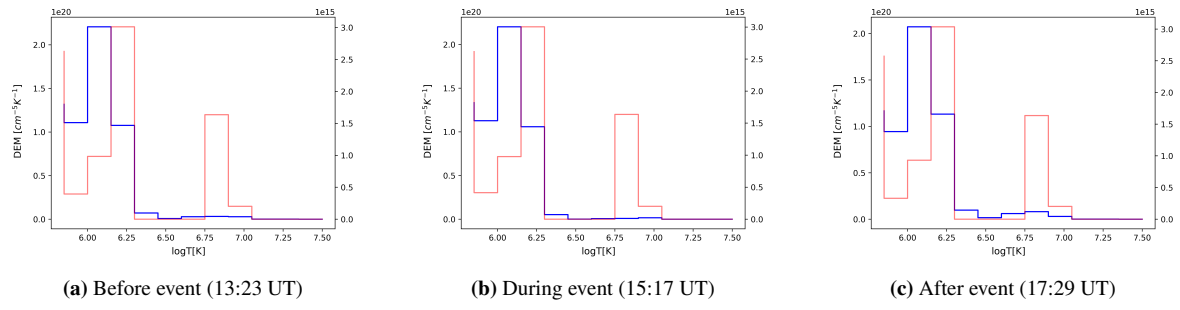


Figure 20: DEM profile before, during and after the flaring event of 28th October 2021. The red and blue curves correspond to point source and full disk source respectively

References

- Aschwanden, M. (2006). *Physics of the solar corona: An introduction with problems and solutions*. Springer Berlin Heidelberg. <https://books.google.co.in/books?id=P2gQwrSbGOgC>
- Athiray, P. S., & Winebarger, A. R. (2024). Can emission measure distributions derived from extreme-ultraviolet images accurately constrain high-temperature plasma? *The Astrophysical Journal*, 961(2), 181. <https://doi.org/10.3847/1538-4357/ad1837>
- Cheung, M. C. M., Boerner, P., Schrijver, C. J., Testa, P., Chen, F., Peter, H., & Malanushenko, A. (2015). Thermal diagnostics with the atmospheric imaging assembly on board the solar dynamics observatory: A validated method for differential emission measure inversions. *The Astrophysical Journal*, 807(2), 143. <https://doi.org/10.1088/0004-637x/807/2/143>
- Gopalswamy, N. (2016). History and development of coronal mass ejections as a key player in solar terrestrial relationship. *Geosci. Lett.*, 3(1).
- Hannah, I. G., & Kontar, E. P. (2012). Differential emission measures from the regularized inversion of hinode and sdo data. *Astronomy amp; Astrophysics*, 539, A146. <https://doi.org/10.1051/0004-6361/201117576>
- Klein, K.-L., Musset, S., Vilmer, N., Briand, C., Krucker, S., Francesco Battaglia, A., Dresing, N., Palmroos, C., & Gary, D. E. (2022). The relativistic solar particle event on 28 october 2021: Evidence of particle acceleration within and escape from the solar corona. *Astronomy amp; Astrophysics*, 663, A173. <https://doi.org/10.1051/0004-6361/202243903>
- Korhonen, H., Vida, K., Leitzinger, M., Odert, P., & Kovacs, O. E. (2016). Hunting for stellar coronal mass ejections.
- Lemen, J. R., Title, A. M., Akin, D. J., Boerner, P. F., Chou, C., Drake, J. F., Duncan, D. W., Edwards, C. G., Friedlaender, F. M., Heyman, G. F., Hurlburt, N. E., Katz, N. L., Kushner, G. D., Levay, M., Lindgren, R. W., Mathur, D. P., McFeaters, E. L., Mitchell, S., Rehse, R. A., ... Waltham, N. (2011). The atmospheric imaging assembly (aia) on the solar dynamics observatory (sdo). *Solar Physics*, 275(1–2), 17–40. <https://doi.org/10.1007/s11207-011-9776-8>
- Mason, J. P., Woods, T. N., Caspi, A., Thompson, B. J., & Hock, R. A. (2014). Mechanisms and observations of coronal dimming for the 2010 august 7 event. *The Astrophysical Journal*, 789(1), 61. <https://doi.org/10.1088/0004-637x/789/1/61>
- Mason, J. P., Woods, T. N., Webb, D. F., Thompson, B. J., Colaninno, R. C., & Vourlidas, A. (2016). Relationship of euv irradiance coronal dimming slope and depth to coronal mass ejection speed and mass. *Astrophys. J.*, 830(1), 20.
- Massa, P., Emslie, A. G., Hannah, I. G., & Kontar, E. P. (2023). Robust construction of differential emission measure profiles using a regularized maximum likelihood method. *Astronomy & Astrophysics*, 672, A120. <https://doi.org/10.1051/0004-6361/202345883>
- Morgan, H., & Pickering, J. (2019). Sites: Solar iterative temperature emission solver for differential emission measure inversion of euv observations. *Solar Physics*, 294(10). <https://doi.org/10.1007/s11207-019-1525-4>
- Moschou, S.-P., Drake, J. J., Cohen, O., Alvarado-Gómez, J. D., Garraffo, C., & Fraschetti, F. (2019). The stellar CME–flare relation: What do historic observations reveal? *Astrophys. J.*, 877(2), 105.

- Namekata, K., Maehara, H., Honda, S., Notsu, Y., Nogami, D., & Shibata, K. (2022). Hunting for stellar coronal mass ejections. *Astrophys. J.*, 939(2), 98.
- Namekata, K., Toriumi, S., Airapetian, V. S., Shoda, M., Watanabe, K., & Notsu, Y. (2023). Reconstructing the XUV spectra of active sun-like stars using solar scaling relations with magnetic flux. *Astrophys. J.*, 945(2), 147.
- Otsu, T., & Asai, A. (2024). Multiwavelength sun-as-a-star analysis of the m8.7 flare on 2022 october 2 using h and euv spectra taken by smart/sddi and sdo/eve. *The Astrophysical Journal*, 964(1), 75. <https://doi.org/10.3847/1538-4357/ad24ec>
- Otsu, T., Asai, A., Ichimoto, K., Ishii, T. T., & Namekata, K. (2022). Sun-as-a-star analyses of various solar active events using h spectral images taken by smart/sddi. *The Astrophysical Journal*, 939(2), 98. <https://doi.org/10.3847/1538-4357/ac9730>
- Pesnell, W. D., Thompson, B. J., & Chamberlin, P. C. (2011). The solar dynamics observatory (sdo). *Solar Physics*, 275(1–2), 3–15. <https://doi.org/10.1007/s11207-011-9841-3>
- Plowman, J., Kankelborg, C., & Martens, P. (2013). Fast differential emission measure inversion of solar coronal data. *The Astrophysical Journal*, 771(1), 2. <https://doi.org/10.1088/0004-637x/771/1/2>
- Sinha, S., Srivastava, N., & Nandy, D. (2019). Solar filament eruptions as precursors to flare–cme events: Establishing the temporal connection. *The Astrophysical Journal*, 880(2), 84. <https://doi.org/10.3847/1538-4357/ab2239>
- Su, Y., Veronig, A. M., Hannah, I. G., Cheung, M. C. M., Dennis, B. R., Holman, G. D., Gan, W., & Li, Y. (2018). Determination of differential emission measure from solar extreme ultraviolet images. *Astrophys. J. Lett.*, 856(1), L17.
- Veronig, A. M., Odert, P., Leitzinger, M., Dissauer, K., Fleck, N. C., & Hudson, H. S. (2021). Indications of stellar coronal mass ejections through coronal dimmings.